ChemElectroChem

Articles
doi.org/10.1002/celc.202000911

**Chemistry
Europe**

European Chemical
Societies Publishing

Nitrate Radical Facilitates Indirect Benzyl Alcohol Oxidation on Bismuth(III) Vanadate Photoelectrodes

Bradley D. Terry, John L. DiMeglio, John P. Cousineau, and Bart M. Bartlett*[a]

Bismuth(III) vanadate ($BiVO_4$) films show activity for direct benzyl alcohol ($PhCH_2OH$) oxidation to benzaldehyde (PhCHO) in acetonitrile solvent. Introducing tetrabutylammonium nitrate (Bu_4NNO_3) drastically reduces the overpotential required to generate the PhCHO product while maintaining a high faradaic efficiency (FE) > 90%. $BiVO_4$ corrosion accompanies $PhCH_2OH$ oxidation. However, the presence of nitrate ions (NO_3^-) results in significantly less bismuth- and vanadium-ion leaching (determined by ICP-MS analysis), as well as reduced surface roughening (determined by SEM imaging). In this reaction, it is proposed that rate-determining NO_3^- oxidation generates a highly reactive nitrate radical ($NO_3\cdot$) that reacts with $PhCH_2OH$ by hydrogen-atom abstraction (HAT). NO_3^- is stoichiometrically consumed by the irreversible formation of electrochemically inert HNO_3, characterized by an EC_i mechanism, rather than a catalytic EC' mechanism. In the presence of $PhCH_2OH$, NO_3^- oxidation on $BiVO_4$ becomes more facile; every order of magnitude increase in $PhCH_2OH$ concentration shifts the $NO_3^-/NO_3\cdot$ equilibrium potential negatively by 200 mV. The shift results from the introduction of a consumption pathway for the nitrate radical intermediate via a coupled chemical step with benzyl alcohol. This report is the first example of photo-electrochemical $NO_3\cdot$ generation to initiate indirect $PhCH_2OH$ oxidation.

1. Introduction

Alcohol oxidation to carbonyl compounds is a valuable chemical transformation in academic and industrial settings. Toxic stoichiometric oxidants such as dichromate and permanganate are commonly used to carry out these reactions.[1] An emerging safer route relies on generating stoichiometric chemical oxidant *in situ* through activating inert reagents.[2] Redox mediators fit this criterion nicely, where the oxidation of stable and reversible redox-active species can form reactive radical or ionic intermediates that proceed to oxidize alcohol substrates in a solution-based chemical step.[3] Redox mediators often mitigate sluggish heterogeneous electron-transfer rates, making them useful in a bevy of applications spanning batteries to catalysis.[4] Several platforms coupling the light-absorbing features of earth-abundant and environmentally friendly metal-oxide photocatalysts with the rapid electron-transfer features of redox mediators have emerged, demonstrating cooperativity for selective alcohol oxidation.[5]

N-oxyl couples, such as 2,2,6,6-tetramethyl-1-piperidinyloxy (TEMPO·/TEMPO$^+$), are the most extensively investigated class of redox mediators for applications in catalytic alcohol/aldehyde oxidation due to their highly reversible redox properties.[6] Indirect alcohol oxidation using a mediator has been associated with unique and often desirable product selectivity.[7] Compared to *N*-oxyl mediators, nitrate anion (NO_3^-) is an underexplored mediator for alcohol oxidation that has received renewed attention. The earliest known report of nitrate-mediated alcohol oxidation proposed a hydrogen atom abstraction (HAT) mechanism upon electrochemical generation of nitrate radical ($NO_3\cdot$).[8] More than 30 years later, examples harnessing biphasic media emerged implementing an organic layer to maximize alcohol substrate solubility along with an aqueous layer for $NO_3\cdot$ generation; highly selective formation of aldehyde and ketone products resulted, proposed to operate via HAT at the biphasic interface.[9] Since then, exploitation of $NO_3\cdot$ for catalytic transformations has burgeoned. Recently, a visible-light excited state of Acr$^+$-Mes dye was used to oxidize NO_3^- to $NO_3\cdot$ for use as an oxidant in subsequent chemical reactions.[10] Continuing with light-harvesting examples, our lab demonstrated cooperativity between the $NO_3^-/NO_3\cdot$ couple and valence-band holes on semiconducting CdS nanowires toward indirect alcohol oxidation; this photocatalytic system oxidizes $PhCH_2OH$ to PhCHO with > 99% selectivity in acetonitrile.[11]

This work aims to expand the scope of compatible semiconductor-nitrate systems for alcohol oxidation. $BiVO_4$ films were used as photoanodes in this study, as their activity toward $PhCH_2OH$ oxidation in composite films has been demonstrated.[12] Our experimental design includes a photoelectrochemical cell illuminated with 100 mW cm^{-2} royal blue LED ($\lambda_{max} = 448$ nm) light that matches the band-gap absorption in $BiVO_4$ (2.4 eV).[13] All solutions were prepared in acetonitrile (MeCN) solvent to stymie competitive solvent oxidation (observed in water) and to maximize substrate solubility. $PhCH_2OH$ was used to glean insight into the underlying mechanism responsible for indirect alcohol oxidation enabled by the $NO_3^-/NO_3\cdot$ couple.

[a] B. D. Terry, J. L. DiMeglio, J. P. Cousineau, Prof. B. M. Bartlett
   Department of Chemistry
   University of Michigan
   930 N. University Ave. Ann Arbor, MI 48109-1055 (USA)
   E-mail: bartmb@umich.edu

ChemElectroChem

Articles
doi.org/10.1002/celc.202000911

**Chemistry
Europe**
European Chemical
Societies Publishing

2. Results

BiVO$_4$ electrodes were prepared by a reported method.[14] The band gap energy (Figure S1) and powder X-ray diffraction pattern (Figure S2) confirm phase purity. To determine appropriate conditions for photoelectrochemistry on BiVO$_4$, its native activity for direct PhCH$_2$OH oxidation was assessed using linear sweep voltammetry (LSV). Figure 1 shows LSV traces collected by sweeping from open-circuit potential (−0.8 V to −0.2 V) to +1 V vs ferrocenium/ferrocene (Fc$^{+/0}$) in MeCN solutions of varying PhCH$_2$OH concentration. The LSV data show that as the concentration of PhCH$_2$OH increases, the photocurrent density also increases. A control LSV experiment in the dark (dashed
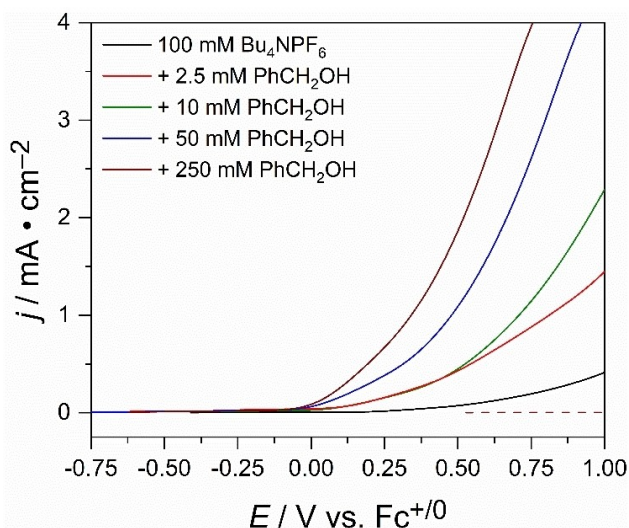
Figure 1. LSV traces on BiVO$_4$ photoelectrodes (1.3 cm^2) collected in acetonitrile solutions containing varying concentrations of PhCH$_2$OH with 100 mM Bu$_4$NPF$_6$ supporting electrolyte. The scan rate is 10 mV s^{-1}. Dashed trace indicates a dark scan.
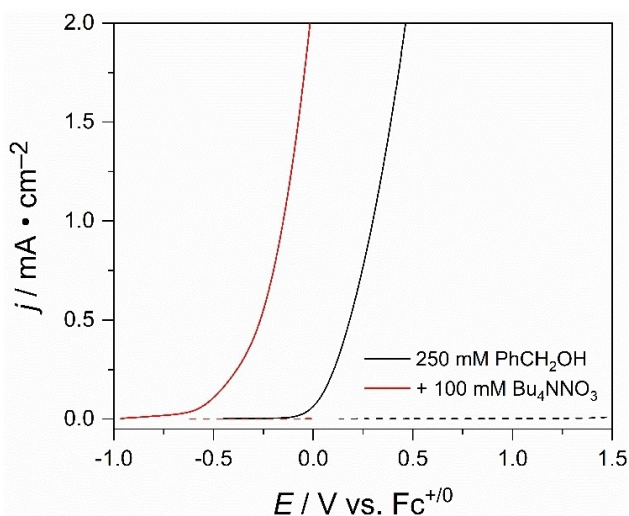
Figure 2. LSVs performed on BiVO$_4$ at 10 mV s^{-1} in acetonitrile solutions containing 100 mM Bu$_4$NPF$_6$ supporting electrolyte with 250 mM PhCH$_2$OH. The effect of adding 100 mM Bu$_4$NNO$_3$ (red trace) is shown. Dashed traces are the dark scans.

trace) supports that this current is indeed derived from photo-generated charge carriers in BiVO$_4$.

To confirm that this anodic current corresponds to PhCH$_2$OH oxidation, we performed controlled potential coulometry (CPC) at 0.75 V vs Fc$^{+/0}$ for 4 hours while stirring the solution to generate enough product for GC-FID analysis. A two-compartment cell with a 1 μm porous glass frit was used to separate the BiVO$_4$ working electrode and reference electrode (Ag wire with Vycor frit) from the Pt coil auxiliary electrode. Figure S3 shows that during the reaction, the current density steadily decreases from 4 mA cm^{-2} to 1 mA cm^{-2}, indicating that BiVO$_4$ is unstable during catalysis (*vide infra*). Nevertheless, PhCHO forms with 88 ± 3 % FE, revealing the native ability for direct PhCH$_2$OH oxidation on BiVO$_4$. With the baseline established, any improvements afforded by indirect oxidation through NO$_3$· generation could be resolved.

Cooperativity between nitrate and BiVO$_4$ was preliminarily detected by LSV. Figure 2 shows that adding 100 mM Bu$_4$NNO$_3$ shifts the photocurrent onset potential negatively by 500 mV. CPC was used to track PhCHO formation in these solutions after a constant 0 V vs Fc$^{+/0}$ potential was applied (Figure S4); direct alcohol oxidation without Bu$_4$NNO$_3$ is exceedingly slow under these conditions (j_{ph} < 0.05 mA cm^{-2}). With Bu$_4$NNO$_3$, the corresponding GC-FID product analysis shows high selectivity for PhCHO (FE = 91 ± 11 %) along with a substantial increase in the amount of PhCHO produced. Although having nitrate in solution leads to faster rates of PhCH$_2$OH oxidation, the photocurrent density steadily decreases over the course of the CPC experiment. Inductively coupled plasma mass spectrometry (ICP-MS) was used to track BiVO$_4$ dissolution. Table 1 shows metal-ion leaching data for several CPC experiments. For the same quantity of charge passed, when more positive potentials were applied – to effect direct PhCH$_2$OH oxidation – higher concentrations of bismuth and vanadium leach into solution. When indirect PhCH$_2$OH oxidation occurs, enabled by the presence of nitrate, the concentration of dissolved metal ions is lower. Illumination-only and bias-only control reactions demonstrate that metal-ion dissolution is linked to catalysis rather than any inherent chemical incompatibility between the supporting electrolyte solution and BiVO$_4$.

Top-down scanning electron microscopy (SEM) images in Figure 3 link the metal-ion leaching to surface roughening on BiVO$_4$ films. Films show significant roughening for direct PhCH$_2$OH oxidation by valence-band holes, where large positive bias is required without nitrate. The morphology change on BiVO$_4$ is dampened when a less positive bias is employed to oxidize PhCH$_2$OH indirectly, enabled by the NO$_3^-$/NO$_3$· couple.

Table 1. Changes in metal-ion concentration after CPC experiments.

| CPC reaction conditions	Δ[Bi] [μM]	Δ[V] [μM]
448 nm illumination +0.75 V vs. Fc$^{+/0}$, 4 h without Bu$_4$NNO$_3$	13.8	14.2
448 nm illumination +0 V vs. Fc$^{+/0}$, 20 h with Bu$_4$NNO$_3$	1.1	2.3
448 nm illumination only, 72 h	0.7	1.2
0.75 V Fc$^{+/0}$ applied bias only, 4 h	0	0
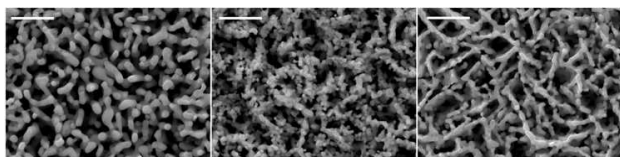
Figure 3. SEM images of a synthesized $BiVO_4$ film (left); film after direct $PhCH_2OH$ oxidation (middle); and after indirect $PhCH_2OH$ oxidation enabled by the $NO_3^-/NO_3\cdot$ couple (right). The scale bar represents 1 μm.

These SEM images compare changes in $BiVO_4$ for the same quantity of charge passed. XPS analysis reveals a shift in the Bi $4f_{7/2}$ and V $2p_{3/2}$ doublet peaks of prepared $BiVO_4$ (158.9 eV and 516.5 eV respectively) to higher binding energies after CPC (159.2 eV and 516.7 eV), indicating a change in surface composition (Figure S5). Although $BiVO_4$ photoanodes show an apparent compositional sensitivity to applied bias, other factors may explain this trend. Alcohol oxidation requires deprotonation, and, like many metal oxides, $BiVO_4$ shows sensitivity to high proton activity.[15] We postulate that NO_3^-, a weak base in acetonitrile ($pK_a \sim 9$),[16] may reduce the extent of photocorrosion.

To understand how added nitrate participates in this indirect cooperative process, we studied the photocurrent dependence on $[Bu_4NNO_3]$ concentration through LSV in MeCN. Figure 4a displays a plateau current that increases in magnitude and shifts to more positive potentials with increasing nitrate concentration. The plateau corresponds to NO_3^- oxidation, and the concentration-dependent plateau potential shift results from the quasi-reversibility in the $NO_3^-/NO_3\cdot$ couple. Next, we introduced varying quantities of $PhCH_2OH$ to solutions containing 10 mM Bu_4NNO_3. Figure 4b shows that the peak current for NO_3^- oxidation is constant (~ 1.7 mA cm^{-2}), but the plateau onset potential shifts to more negative potentials as the $PhCH_2OH$ concentration increases. The observation of a plateau in the photocurrent density reveals that indirect $PhCH_2OH$ oxidation does not regenerate NO_3^-. Instead, $NO_3\cdot$ reacts irreversibly (i.e. stoichiometrically) through an EC_i mechanism. The expected regeneration of NO_3^- through a catalytic EC' mechanism does not occur. The photocurrent dependence on the scan rate in Figure 5 also supports an EC_i mechanism; the peak current density depends on the square root of scan rate ($j_p \propto v^{0.5}$), as predicted by the Randles-Sevcik equation.[17] The anodic peaks observed for fast scan rates ($v \geq 50$ mV s^{-1}) correspond to depletion of NO_3^- at the photoanode surface that would not occur under catalytic regeneration.[18] The shifting peak potential with increasing scan rate is also characteristic of irreversible NO_3^- oxidation.

Along with a stoichiometric consumption of NO_3^-, we observe a shift in the onset potential for NO_3^- oxidation when $PhCH_2OH$ is present. The facilitation of NO_3^- oxidation by $PhCH_2OH$ in the LSV traces is linked to faster rates of $PhCH_2OH$ oxidation (forming PhCHO) confirmed by CPC experiments. The plot in Figure 6 shows a slope of ~ 200 mV per order of magnitude increase in $PhCH_2OH$ concentration. For a reversible redox couple, the Nernst equation predicts a 59.1 mV shift per
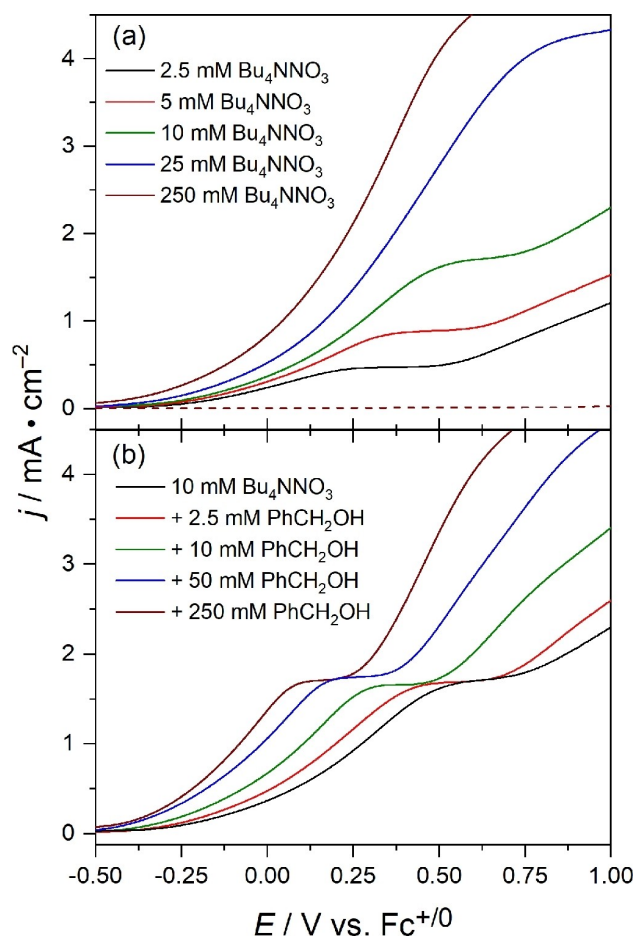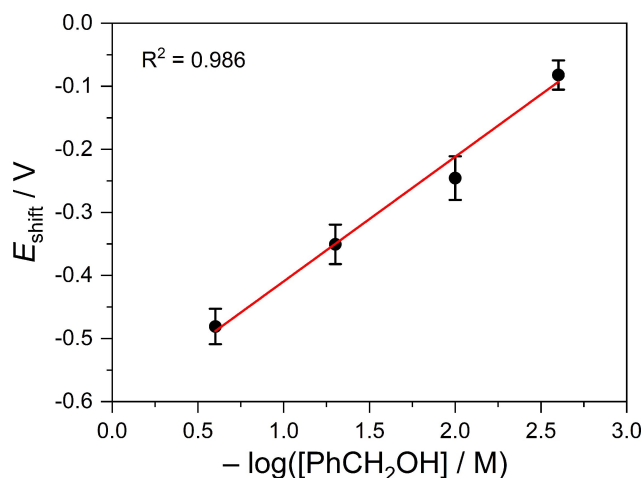

Figure 4. LSV traces collected on $BiVO_4$ in MeCN solutions containing 100 mM Bu_4NPF_6 supporting electrolyte with varying concentrations of Bu_4NNO_3. Dashed lines represent the dark scans (a). LSV traces of varying $PhCH_2OH$ concentrations in a 10 mM Bu_4NNO_3 solution with supporting electrolyte (b). All LSVs were collected at 10 mV s^{-1}.
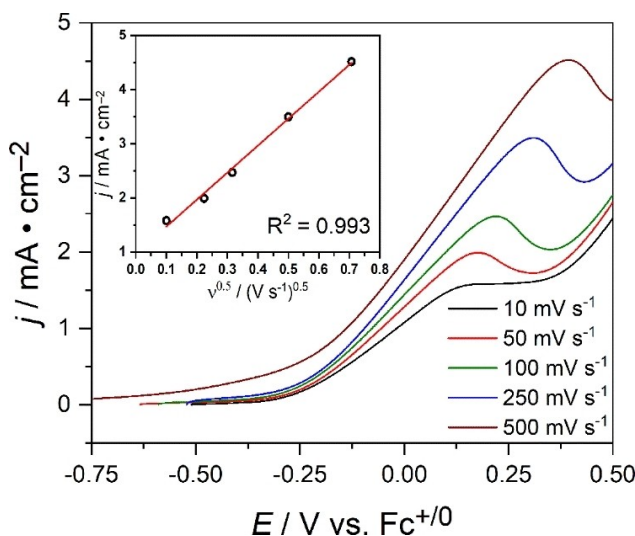
Figure 5. Scan-rate-dependent LSV traces on $BiVO_4$ in MeCN solution containing 10 mM Bu_4NNO_3 and 250 mM $PhCH_2OH$ with Bu_4NPF_6 supporting electrolyte. The inset shows the linear fit for peak photocurrent density as a function of the square root of scan rate.
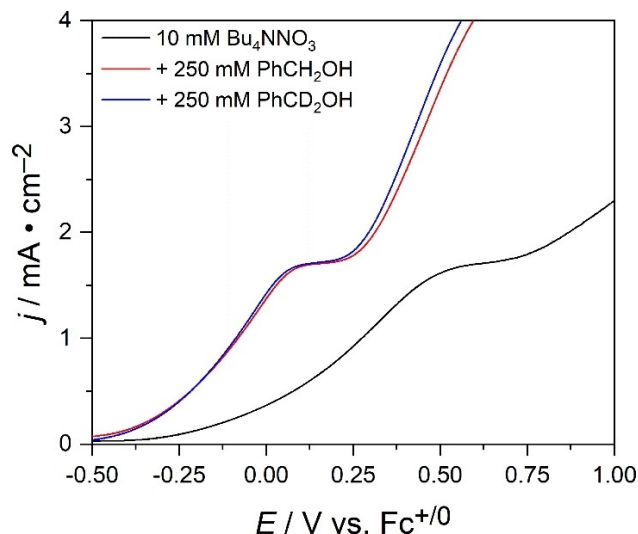
ChemElectroChem

Articles
doi.org/10.1002/celc.202000911

Chemistry
Europe
European Chemical
Societies Publishing

Figure 6. Shift in potential corresponding to the center of the plateau for NO_3^- oxidation ($j = 1.6$ mA cm^{-2}–1.7 mA cm^{-2}) as a function of $-\log$[PhCH$_2$OH] in 10 mM Bu$_4$NNO$_3$ solution.

order of magnitude increase in substrate concentration.[16] The quasi-reversible nature of the NO_3^-/$NO_3\cdot$ couple results in a much larger equilibrium potential shift due to a substrate-driven consumption pathway for $NO_3\cdot$.

Reduced photocorrosion on BiVO$_4$ and irreversible NO_3^- oxidation (Figure 4b) point toward a reaction between $NO_3\cdot$ and PhCH$_2$OH proceeding through HAT to yield HNO$_3$. Consequently, the concentration of $NO_3\cdot$ at the BiVO$_4$ photoelectrode surface decreases and this perturbation of equilibrium concentrations for NO_3^- and $NO_3\cdot$ creates a driving force to reestablish equilibrium (Le Chatelier's principle); this driving force is measured as the shift in Figure 6.

To investigate irreversible nitrate consumption coupled to alcohol oxidation further, isotopic rate studies were performed. Figure 7 shows nearly identical LSV responses when using (α,α-
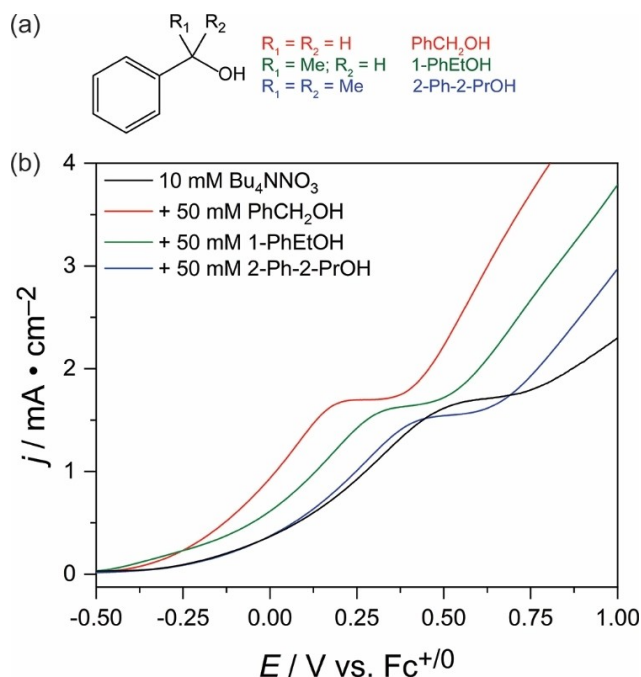
d_2) deuterated PhCD$_2$OH under the same conditions, revealing no 1° kinetic isotope effect (KIE). This result indicates that the α-hydrogen does not react in the rate-determining step. However, this observation does not rule out a stepwise process involving rate-determining NO_3^- oxidation followed by a fast HAT step consuming $NO_3\cdot$ and yielding HNO$_3$. In acetonitrile, the weak electrolyte HNO$_3$ is inert toward indirect PhCH$_2$OH oxidation on BiVO$_4$ photoelectrodes (Figures S6 and S7).

To probe further the reaction between $NO_3\cdot$ and alcohol substrate in solution, we compared the LSV traces within the series of α-methylated benzyl alcohol derivatives. The green trace of Figure 8 shows that the secondary alcohol, 1-phenyl-ethanol results in a diminished shift for the NO_3^-/$NO_3\cdot$ couple. Steric hindrance about the benzylic carbon appears to slow down reactivity between $NO_3\cdot$ and alcohol substrate.

Continuing with the series, one would expect that $NO_3\cdot$ reacting through HAT would indeed require an α-hydrogen. Not surprisingly, when the tertiary alcohol, 2-phenyl-2-propanol is introduced, a reversion to substrate-free nitrate behavior is observed (Figure 8, blue trace). The potential at which the photocurrent begins to plateau progressively shifts approximately 100 mV to more positive values as the benzylic carbon becomes increasingly methylated: ~ 0.20 V, 0.30 V, 0.40 V vs. Fc$^{+/0}$ for BnOH, 1-PhEtOH, and 2-Ph-2-PrOH respectively. This shift highlights the role of the α-hydrogen in this EC$_i$ mechanism.[8][9][11]

Figure 7. Illuminated LSV traces comparing 250 mM PhCH$_2$OH oxidation (red) and 250 mM PhCD$_2$OH oxidation (blue) with 10 mM Bu$_4$NNO$_3$ in MeCN containing 100 mM Bu$_4$NPF$_6$ supporting electrolyte. The scan rate is 10 mV s^{-1}.

Figure 8. a) Series of benzyl alcohol derivatives used in this study. b) LSV traces comparing benzyl alcohol and its derivatives. Solutions contain 50 mM alcohol, 10 mM Bu$_4$NNO$_3$ and 100 mM Bu$_4$NPF$_6$ supporting electrolyte in MeCN. The scan rate is 10 mV s^{-1}.

ChemElectroChem

Articles
doi.org/10.1002/celc.202000911

**Chemistry
Europe**
European Chemical
Societies Publishing

3. Discussion

Scheme 1 presents the mechanistic picture that unfolds from the experimental observations. Herein, we demonstrate the native activity for direct PhCH$_2$OH oxidation on BiVO$_4$ and show the substantial rate improvement afforded by coupling to NO$_3^-$ oxidation. Optimized conditions (Figure S8) show high faradaic efficiency – $99 \pm 9\%$ – for benzaldehyde product through indirect electron transfer. Importantly, photoelectrochemically oxidizing NO$_3^-$ on BiVO$_4$ in the first mechanistic step enables indirect alcohol oxidation at potentials where direct alcohol oxidation does not occur. NO$_3^-$ oxidation shows quasi-reversible kinetics, evidenced by a shifting peak current density (Figure 5) and a non-Nernstian 200 mV shift in the NO$_3^-$/NO$_3\cdot$ equilibrium potential per order of magnitude increase in PhCH$_2$OH concentration (Figure 6). An irreversible chemical step perturbs the equilibrium concentration of NO$_3^-$/NO$_3\cdot$ due to a consumption pathway for NO$_3\cdot$ that affords the desired PhCHO product.
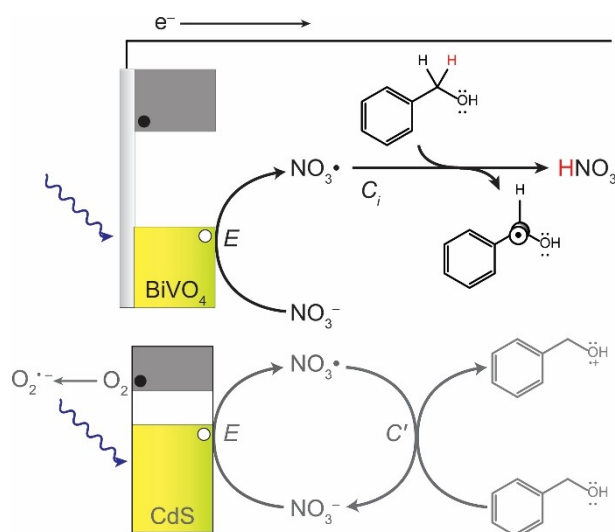

Scheme 1. Observed EC$_i$ mechanism for indirect PhCH$_2$OH oxidation through NO$_3\cdot$ on BiVO$_4$ photoelectrodes (top). Alternate EC' mechanism observed on CdS nanowires (bottom).

Previous work in our lab demonstrates that NO$_3^-$ acts as a redox mediator (i.e. it is regenerated) in photocatalytic PhCH$_2$OH oxidation on CdS nanowires.[11] Photoelectrochemically, NO$_3^-$ is not regenerated, representing an EC$_i$ mechanism. The difference in NO$_3^-$ behavior in the two acetonitrile systems is rationalized in the context of the full light-driven redox cycle. On CdS nanowires, electrons are photoexcited to the conduction band, where they carry out the oxygen reduction reaction. If that reaction is carried out under inert N$_2$ atmosphere, PhCH$_2$OH oxidation is slow, and NO$_3^-$ is consumed (likely by its reduction). Reduced oxygen species, such as superoxide (O$_2^-$), that are co-located with either HNO$_3$ or a carbon-centered radical intermediate can deprotonate HNO$_3$ after HAT or avoid HNO$_3$ formation altogether, rendering NO$_3^-$ catalytic. In photoelectrochemistry, these reactions occur in separate compartments such that NO$_3^-$ oxidation on a BiVO$_4$ working electrode is separated – by several centimeters – from the reduction reactions on the platinum auxiliary electrode. Accordingly, carrying out the photoelectrochemical reaction on BiVO$_4$ anaerobically (under N$_2$) shows no discernable difference in the voltammetric response (Figure S9), demonstrating that reduced oxygen species such as O$_2^-$ do not act as a base is under these conditions. Rather, nitrate in the working compartment is the only local base.

Neither CdS nanowire photocatalysis nor BiVO$_4$ photoelectrochemistry show a 1° KIE for PhCH$_2$OH/PhCD$_2$OH oxidation. On BiVO$_4$, NO$_3^-$ consumption and lack of KIE point to rate-determining NO$_3^-$ oxidation with a fast HAT step. The voltammetric response of a series the para-substituted benzyl alcohol derivatives, 4-chlorobenzyl alcohol and 4-tert-butylbenzyl alcohol was measured (Figure S10), and the zero slope in the data reveal no buildup of charge in the transition state. While electronic factors have a negligible influence on the rate of indirect alcohol oxidation using photoelectrochemically generated NO$_3\cdot$, the functionality about the benzylic position (Figure 8) has substantial impact.

Density functional theory also helps distinguish between HAT and single-electron transfer (SET) mechanisms. Figure 9 shows the frontier orbitals energies and projections of the HOMO of PhCH$_2$OH and the derivatives described throughout
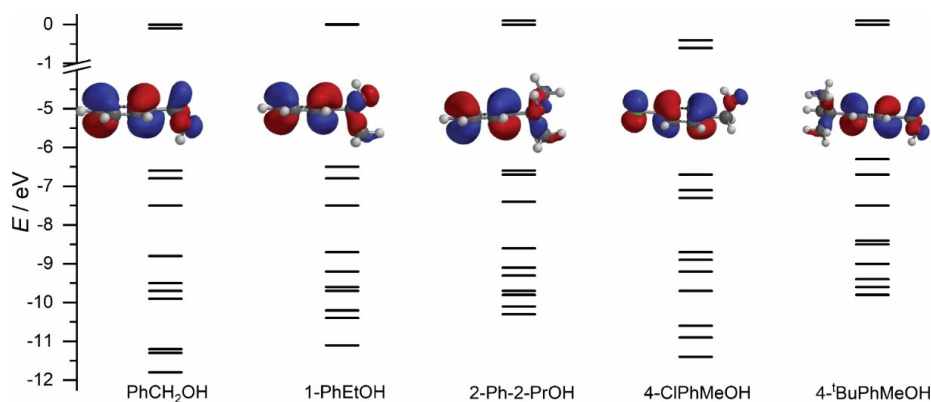
Figure 9. DFT calculations (B3LYP functionals, 6–31G* basis set) of the frontier orbitals of benzyl alcohol and its derivatives; the projection of the HOMO illustrated.

ChemElectroChem

Articles
doi.org/10.1002/celc.202000911

Chemistry
Europe
European Chemical
Societies Publishing

the manuscript. Of note, the HOMO of benzyl alcohol has aromatic π* and oxygen 2p lone-pair character with an energy −6.6 eV. As the number of methyl groups increases, the HOMO adds slight C−C σ bonding character and the energy *increases slightly* or is unchanged: −6.5 eV for 1-PhEtOH and −6.6 eV for 2-Ph-2-PrOH. Taking the HOMO energy as an approximation for ionization energy by Koopman's theorem[19] and adding the dielectric continuum to account for solvation energies, we would predict that if SET were the operative mechanism, then the potential at which the anodic current plateaus would be nearly constant (if not show a slight shift to more *negative* values). The observed shift to more positive potentials suggests a HAT mechanism that forms a carbon-centered radical opposed to SET that forms an oxygen-centered radical. Moreover, the HOMO energies for the para-substituted derivatives remain similar, −6.7 eV for 4-chlorobenzyl alcohol and −6.3 eV for 4-*tert*-butylphenyl methanol.

For reversible redox couples, the Nernst equation predicts a 59.1 mV equilibrium potential shift per order of magnitude increase in substrate concentration. This theoretical treatment was demonstrated empirically in a recent report describing a $TEMPO^+-N_3^-$ system.[20] TEMPO radical oxidation was facilitated in the presence of N_3^- by forming a stable charge-transfer complex, which showed a 62 mV shift per order of magnitude increase in $[N_3^-]$. In our work, NO_3^- is not regenerable on BiVO$_4$ and the 200 mV potential shift slope (Figure 6) is non-Nernstian due to the quasi-reversibility of the $NO_3^-/NO_3\cdot$ couple as well as an irreversible chemical step (EC$_i$) where nitrate radical is consumed; introducing a benzyl alcohol-based consumption pathway vastly improves the electrochemical kinetics for NO_3^- oxidation.

Another key difference between the two acetonitrile systems is the importance of nitrate's counterion in the salt. We find Bu$_4$NNO$_3$ to be a viable source of nitrate for indirect alcohol oxidation on BiVO$_4$. However, Bu$_4$NNO$_3$ does not mediate photocatalytic PhCH$_2$OH oxidation on CdS nanowires. There, a hard metal cation such as Li$^+$, Ca^{2+}, or Mn^{2+} is required, and metal-cation coordination with nitrate is observed by both UV-Vis and FTIR spectroscopy. Absorption features for NO_3^- ($n\rightarrow\pi^*$) show a blue shift in acetonitrile with metal cations present; this perturbation in electronic structure suggests an altered redox potential for the $NO_3^-/NO_3\cdot$ couple. Therefore, the lack of general activity in acetonitrile using Bu$_4$NNO$_3$ supports misalignment between the redox potential $E(NO_3^-/NO_3\cdot)$ and the valence band edge (E_{VB}) of CdS. A similar thermodynamic mismatch was discovered recently between TEMPO and BiVO$_4$ photoanodes in water.[21] There, TEMPO was shown to act as a recombination center, hindering electron transfer from BiVO$_4$ to solution; tuning the surface-mediator interaction with an interfacial cobalt phosphate layer enabled TEMPO mediation. In that example, a heterogeneous treatment was used to overcome redox potential-band edge misalignment, and we postulate that metal cations in solution address the issue on CdS.

Recently, a report detailing indirect PhCH$_2$OH oxidation in aqueous electrolyte showed selective generation of PhCHO on BiVO$_4$ photoanodes decorated with a layered double hydroxide (LDH) surface electrocatalyst.[22] In that system, indirect alcohol oxidation was achieved through a surface-bound hydroxyl radical intermediate generated from water oxidation on the cobalt-based LDH. Comparison of this system with our work reveals key similarities, namely the formation of a carbon-centered benzyl alcohol radical and stoichiometric consumption of a radical intermediate ($\cdot OH/NO_3\cdot$). While both systems function through an EC$_i$ mechanism, the consumption of $NO_3\cdot$ through HAT is responsible for forming the benzyl alcohol radical, while the LDH@BiVO$_4$ system forms the benzyl alcohol radical through an activation step *before* $\cdot OH$ reacts. Nevertheless, both systems show accelerated rates for PhCH$_2$OH oxidation upon introducing indirect pathways characterized as "radical relays." Exploring the scope of radical relays and their role in catalyzing alcohol oxidation reactions is the subject of ongoing investigation in our lab.

4. Conclusions

We show that nitrate anion effects indirect photoelectrochemical benzyl alcohol oxidation on bismuth(III) vanadate in acetonitrile solvent. The applied potential required to generate benzaldehyde was reduced by ~500 mV, while retaining >90% high faradaic efficiency. The coupled chemical step of benzyl alcohol substrate oxidation leads to faster electrochemical nitrate anion oxidation; the shift is 200 mV per order of magnitude increase in alcohol substrate concentration. The chemical step is likely rapid nitrate radical consumption through hydrogen-atom transfer with benzyl alcohol to yield nitric acid. Deuterating the alpha positions (benzyl alcohol α,α-d$_2$) shows no change in reaction rate, supporting that nitrate anion oxidation is rate-determining and distinct. Lower applied potentials to generate benzaldehyde product and diminished bismuth vanadate photocorrosion are significant benefits granted with nitrate anion reactant.

Conflict of Interest

The authors declare no conflict of interest.

[1] H. Li, F. Qin, Z. Yang, X. Cui, J. Wang, L. Zhang, *J. Am. Chem. Soc.* **2017**, *139*, 3513–3521.

[2] K. Sayama, *ACS Energy Lett.* **2018**. *3*, 1093–1101.

[3] R. Dao, C. Zhao, J. Yao, H. Li, *Phys. Chem. Chem. Phys.* **2018**, *20*, 28249–28256.

[4] a) H.-J. Peng, G. Zhang, X. Chen, Z.-W. Zhang, W.-T. Xu, J.-Q. Huang, Q. Zhang, *Angew. Chem. Int. Ed.* **2016**, *55*, 12990–12995; *Angew. Chem.* **2016**, *128*, 13184–13189; b) Y. Chen, S. A. Freunberger, Z. Peng, O. Fontaine, P. G. Bruce, *Nat. Chem.* **2013**, *5*, 489–494; c) Z. Luo, Y. V. Geletii, D. A. Hillesheim, Y. Wang, C. L. Hill, *ACS Catal.* **2011**, *1*, 1364–1370; d) A. Badalyan, S. S. Stahl, *Nature*, **2016**, *535*, 406–410.

[5] a) H. G. Cha, K.-S. Choi, *Nat. Chem.* **2015**, *7*, 328–333; b) T. Li, T. Kasahara, J. He, K. E. Dettelbach, G. M. Sammis, C. P. Berlinguette, *Nat. Commun.* **2017**, *8*, 390.

[6] a) A. Badalyan, S. S. Stahl, *Nature.* **2016**, *535*, 406–410; b) M. B. Lauber, S. S. Stahl, *ACS Catal.* **2013**, *3*, 2612–2616; c) A. E. J. De Nooy, A. C. Besemer, H. van Bekkum, *Tetrahedron.* **1995**, *51*, 8023–8032; d) B. J. Taitt, M. T. Bender, K.-S. Choi, *ACS Catal.*, **2020**, *10*, 265–275.

[7] a) A. Rahimi, A. Azaripa, H. Kim, J. Ralph, S. S. Stahl, *J. Am. Chem. Soc.* **2013**, *135*, 6415–6418; b) A. E. J. De Nooy, A. C. Besemer, H. van Bekkum, *Carbohydr. Res.* **1995**, *269*, 89–98.

[8] J. E. Leonard, P. C. Scholl, T. P. Steckel, S. E. Lentsch, M. R. Van De Mark, *Tetrahedron Lett.* **1980**, *21*, 4695–4698.

[9] a) C. Christopher, S. Lawrence, M. A. Kulandainathan, K. Kulangiappar, M. E. Raja, N. Xavier, S. Raja, *Tetrahedron Lett.* **2012**, *53*, 2802–2804; b) C. Christopher, S. Lawrence, A. J. Bosco, N. Xavier, S. Raja, *Catal. Sci. Technol.* **2012**, *2*, 824–827.

[10] T. Hering, T. Slanina, A. Hancock, U. Wille, B. König, *Chem. Commun.* **2015**, *51*, 6568–6571.

[11] J. L. DiMeglio, A. G. Breuhaus-Alvarez, S. Li, B. M. Bartlett, *ACS Catal.* **2019**, *9*, 5732–5741.

[12] H. Tateno, Y. Miseki, K. Sayama, *ChemElectroChem.* **2017**, *4*, 3283–3287.

[13] K. Sivula, R. Van De Krol, *Nat. Rev. Mater.* **2016**, *1*, 15010.

[14] T. W. Kim, K.-S. Choi, *Science*, **2014**, *343*, 990–994.

[15] L. Han, P. Tang, A. Reyes-Carmona, Rodríguez-García, M. Torréns, J. R. Morante, J. Arbiol, J. R. Galan-Mascaros, *J. Am. Chem. Soc.* **2016**, *138*, 16037–16045.

[16] F. Eckert, I. Leito, A. Kütt, A. Klamt, M. Diedenhofen, *J. Comput. Chem.* **2009**, *30*, 799–810.

[17] N. Elgrishi, K. J. Rountree, B. D. McCarthy, E. S. Rountree, T. T. Eisenhart, J. L. Dempsey, *J. Chem. Educ.* **2018**, *95*, 197–206.

[18] V. C.-C. Wang, B. A. Johnson, *ACS Catal.* **2019**, *9*, 7109–7123.

[19] T. Koopmans, *Physica* **1934**, *1*, 104–113.

[20] J. C. Siu, G. S. Sauer, A. Saha, R. L. Macey, N. Fu, T. Chauviré, K. M. Lancaster, S. Lin, *J. Am. Chem. Soc.* **2018**, *140*, 12511–12520.

[21] D. J. Chadderdon, L.-P. Wu, Z. A. McGraw, M. Panthani, W. Li, *ChemElectroChem.* **2019**, *6*, 3387–3392.

[22] L. Luo, Z.-J. Wang, X. Xiang, D. Yan, J. Ye, *ACS Catal.* **2020**, *10*, 4906–4913.